Catalysis
Science & Technology

RSC Publishing

PAPER

Enhanced low-temperature activity of CO_2 methanation over highly-dispersed Ni/TiO_2 catalyst†

Cite this: *Catal. Sci. Technol.*, 2013, **3**, 2627

Jie Liu, Changming Li, Fei Wang, Shan He, Hao Chen, Yufei Zhao, Min Wei,* David G. Evans and Xue Duan

Received 22nd May 2013,
Accepted 27th June 2013

DOI: 10.1039/c3cy00355h

www.rsc.org/catalysis

The sustainable development of carbon recycling has attracted considerable attention from the viewpoint of the environment and resources. Herein, Ni nanoparticles (NPs) immobilized on a TiO_2 support were synthesized *via* a deposition–precipitation method followed by a calcination–reduction process (denoted as Ni/TiO_2-DP), which can be used as a promising heterogeneous catalyst towards CO_2 methanation. Transmission electron microscope (TEM) images show that Ni NPs are highly dispersed on the TiO_2 surface (particle size: 2.2 nm), with a low Ni–Ni coordination number revealed by the hydrogen temperature programmed desorption (H_2-TPD) and extended X-ray absorption fine structure (EXAFS) techniques. Moreover, the catalyst with a Ni loading of 15 wt% exhibits excellent catalytic behavior towards CO_2 methanation (conversion: 96%; selectivity: 99%) at a reaction temperature as low as 260 °C. The good dispersion of Ni NPs with large unsaturation facilitates a high exposure of active sites, which accelerates the formation of surface-dissociated hydrogen and the subsequent hydrogenation removal of surface nickel carbonyl species, accounting for the resulting enhanced low-temperature catalytic performance.

1. Introduction

The ever-increasing emissions of carbon dioxide into the atmosphere, considered as the major cause of global warming, have increasingly aroused worldwide concern.[1–3] The catalytic hydrogenation of carbon dioxide to give methane, known as CO_2 methanation, is one of the efficient approaches to recycle CO_2 emissions to give a useful fuel, with potential commercial applications and environmental benefits.[4–8] Noble metals (*e.g.*, Ru, Rh, Pd) supported on various oxide supports (*e.g.*, SiO_2, Al_2O_3, ZrO_2, CeO_2) have been found to be the most effective catalysts for CO_2 methanation at relatively mild operating conditions,[9–15] but the high cost as well as their limited availability restrict their practical applications.[16–19] Therefore, increasing attention has recently been focused on non-noble metal catalysts (*e.g.*, Ni, Co, Cu) for the purpose of obtaining a feasible and cost-effective catalytic process.[4,20–23]

Nickel-based heterogeneous catalysts are the most widely studied system towards CO_2 hydrogenation, but a high activation temperature (above 350 °C) is generally needed to achieve the maximum CO_2 conversion, which results in undesirable influences on the stability/lifetime of the catalysts as well as increased energy consumption.[9,24,25] Therefore, extensive investigations have been conducted to improve the low-temperature catalytic activity for Ni-based catalysts (*e.g.*, Ni–Zr alloys,[17,26,27] Ni–Al alloys[28,29] and RANEY® Ni catalysts[30]), but their low-temperature activity is still to be enhanced further. One major problem that restrains their low-temperature behavior is the deactivation of Ni-based catalysts at low temperature, as a result of the interaction of the metal particles with CO and the formation of mobile nickel subcarbonyls.[31] A key step for the promotion of catalytic activity is the fast removal of this surface nickel carbonyls by surface-dissociated hydrogen.[32,33] It has been reported that the surface defects of metallic Ni serve as capture traps for surface hydrogen diffusion which reduces the activation energy of hydrogen dissociation.[34–37] Moreover, largely enhanced surface defects can be achieved by decreasing the supported particles into the nano-scale with a simultaneous high dispersion.[38,39] Therefore, it is proposed that a Ni-based catalyst would show significantly improved activity by introducing abundant surface defects, so as to generate surface-dissociated hydrogen for the removal of surface nickel carbonyls and consequently promote the low-temperature performance towards CO_2 methanation.

In this work, Ni nanoparticles immobilized on a TiO_2 support were synthesized *via* a deposition–precipitation

State Key Laboratory of Chemical Resource Engineering, Beijing University of Chemical Technology, Beijing, 100029, China. E-mail: weimin@mail.buct.edu.cn; Fax: +86-10-64425385; Tel: +86-10-64412131

† Electronic supplementary information (ESI) available. See DOI: 10.1039/c3cy00355h

method (denoted as Ni/TiO_2-DP) followed by a calcination–reduction process, and these were then used for the hydrogenation of carbon dioxide to methane. The TEM image shows that the Ni NPs are highly dispersed on the TiO_2 surface with a uniform size of 2.2 nm for the Ni(15%)/TiO_2-DP sample, much smaller than the sample prepared by the conventional impregnation method (5.8 nm). Hydrogenation temperature programmed reduction (H_2-TPR) and XPS reveal that a highly-dispersed Ni species comes into formation with a strong metal–support interaction. Extended X-ray absorption fine structure (EXAFS) and hydrogenation temperature programmed desorption (H_2-TPD) demonstrate that the supported Ni NPs on TiO_2 possess a high level of unsaturation, and provide more catalytic active sites that contribute to generating surface-dissociated hydrogen. The Ni(15%)/TiO_2-DP catalyst exhibits the significantly enhanced low-temperature activity (conversion: 96%; selectivity: 99%) and satisfactory stability. Therefore, this work provides a facile approach for the preparation of highly-dispersed Ni NPs catalyst, which can be potentially used as a promising candidate in CO_2 methanation.

2. Experimental section

2.1 Materials

The TiO_2 (P25) and $Ni(NO_3)_2{\cdot}6H_2O$ were purchased from Sigma-Aldrich. Deionized water was used in all the experimental processes.

2.2 Catalyst preparation

The Ni(5%)/TiO_2 catalyst with a Ni loading of 5 wt% was prepared by the precipitation–deposition method. Firstly, titanium dioxide (P25) 3.0 g was dried overnight in an oven at 180 °C and added into 60 mL deionized water under stirring. Then the pH of the resulting suspension was adjusted to 8.0 with $NH_3{\cdot}H_2O$ aqueous solution (0.1 M). Subsequently, $Ni(NO_3)_2{\cdot}6H_2O$ aqueous solution (20 mL, 0.128 M) was added dropwise into the above suspension and the resulting green suspension was aged at room temperature for 3 h with stirring. The precipitation obtained was separated by centrifugation, washed with water three times and dried at 110 °C for 4 h, followed by calcination in air at 400 °C for 3 h with a heating rate of 5 °C min^{-1} and the obtained sample was denoted as NiO(5%)/TiO_2-DP. Samples with different Ni loadings (10 wt%, 15 wt% and 20 wt%) were also prepared by a similar process and were denoted as NiO(10%)/TiO_2-DP, NiO(15%)/TiO_2-DP and NiO(20%)/TiO_2-DP, respectively. Finally, all of the as-calcined NiO/TiO_2-DP samples were reduced in a gasous mixture of H_2 and N_2 (2 : 3, v/v) for 4 h at 450 °C with a heating rate of 5 °C min^{-1}, and the obtained catalysts were denoted as Ni(5%)/TiO_2-DP, Ni(10%)/TiO_2-DP, Ni(15%)/TiO_2-DP and Ni(20%)/TiO_2-DP, respectively.

To investigate the effect of the preparation method on the catalytic performance, the Ni/TiO_2 catalyst with a Ni loading of 15 wt% was also prepared by the conventional impregnation method. Typically, TiO_2 (3.0 g) was added to a $Ni(NO_3)_2{\cdot}6H_2O$ solution (2.2230 g, 5 mL). After agitation for 3 h, the resultant slurry was dried at 110 °C for 4 h, followed by calcination in air at 400 °C for 3 h. The obtained sample was denoted as NiO(15%)/TiO_2-IMP. Finally, the sample was reduced in a gaseous mixture of H_2 and N_2 (2 : 3, v/v) at 450 °C for 4 h with a heating rate of 5 °C min^{-1}, which was denoted as Ni(15%)/TiO_2-IMP.

2.3 Characterization of catalysts

XRD measurements were performed on a Rigaku XRD-6000 diffractometer, using Cu Kα radiation (λ = 0.154 nm) at 40 kV, 30 mA, a 2θ angle ranging from 15° to 80°, and a scanning rate of 10°, a step size of 0.02° s^{-1}. Nickel elemental analysis was performed by atomic emission spectroscopy with a Shimadzu ICPS-7500 instrument. The Ni NPs dispersion was observed using a JEM-2100 high-resolution transmission electron microscope (HRTEM) and the accelerating voltage was 200 kV. EXAFS spectroscopy of the Ni K-edge of the samples was performed at the beam line 1W1B of the Beijing Synchrotron Radiation Facility (BSRF), Institute of High Energy Physics (IHEP), Chinese Academy of Sciences (CAS). The typical energy of the storage ring was 0.8 GeV with a maximum current of 250 mA. The Si (111) double crystal monochromator was used. The data analysis of all the EXAFS spectra was carried out using UWXAFS. Low-temperature N_2 adsorption–desorption experiments were carried out using the Quantachrome Autosorb-1C-VP instrument. Prior to N_2 adsorption, the sample was outgassed at 200 °C overnight to desorb moisture adsorbed on the surface of the sample. H_2-TPR and H_2-TPD were conducted in a quartz tube reactor on a Micromeritics ChemiSorb 2720 with a thermal conductivity detector (TCD). In a typical H_2-TPR process, 100 mg of sample placed in a quartz tube reactor was first degassed under flowing argon at 200 °C for 2 h and cooled down to room temperature. Then a gaseous mixture of H_2 and Ar (1 : 9, v/v) was fed into the reactor at 40 mL min^{-1}. The temperature was raised to 700 °C at a heating rate of 10 °C min^{-1}. For the H_2-TPD process, 100 mg of sample was first sealed and reduced in the reactor in the gaseous mixture of H_2 and Ar (1 : 9, v/v) at 450 °C for 3 h. Subsequently, the reduced sample was purged in Ar at 500 °C for 30 min to remove excess hydrogen, then cooled down to 25 °C for readsorption of H_2; finally, the sample was contained in a stream of argon at a rate of 40 mL min^{-1} and a temperature ramp of 10 °C min^{-1} to perform the TPD. The dispersion of Ni was calculated based on the volume of chemisorbed H_2 using the following simplified equation:[40]

$$D(\%) = \frac{2 \times V_{ad} \times M \times SF}{m \times P \times V_m \times d_r} \times 100 \quad (1)$$

where V_{ad} (mL) denotes the volume of chemisorbed H_2 at standard temperature and pressure (STP) conditions measured in the TPD procedure; m is the weight of sample (g); M is the molecular weight of Ni (58.69 g mol^{-1}); P is the weight fraction of Ni in the sample as determined by ICP; SF is the stoichiometric factor (the Ni : H molar ratio in the chemisorption) which is taken as 1 and V_m is the molar volume of

H_2 (22 414 mL mol^{-1}) at STP; and d_r is the reduction degree of nickel calculated based on H_2-TPR.

2.4 Catalytic evaluation

The catalytic performances of the nickel-based catalysts were evaluated at atmospheric pressure in a fixed-bed quartz reactor with an interior diameter of 8 mm. The reactor was heated in a tube furnace equipped with a temperature controller. All gases were monitored by calibrated mass flow controllers. Prior to the catalytic performance test, 1.0 g of catalyst was first pretreated *in situ* in a gaseous mixture of H_2 and N_2 (2 : 3, v/v) for 4 h with a total gas flow of 100 mL min^{-1} at 450 °C with a heating rate of 5 °C min^{-1}, and then cooled to 150 °C in nitrogen. Subsequently, a mixture of H_2, CO_2 and Ar (an internal standard) with a molar ratio of $H_2 : CO_2 : Ar = 12 : 3 : 5$ was introduced into the reactor and the total flow rate was set to be 40 mL min^{-1}. The gas hourly space velocity (GHSV) was varied between 1800 h^{-1} and 9000 h^{-1} by changing the total flow rate while keeping the catalyst mass constant. The composition of the outlet gases was analyzed online using a GC-2014C gas chromatograph with a TDX-01 column and TCD detector. The CO_2 conversion and CH_4 selectivity are defined as follows:

$$\text{Conversion}_{CO_2}(\%) = \frac{C_{\text{in}\,(CO_2)} - C_{\text{out}\,(CO_2)}}{C_{\text{in}\,(CO_2)}} \times 100 \quad (2)$$

$$\text{Selectivity}_{CH_4}(\%) = \frac{C_{(CH_4)}}{C_{\text{in}\,(CO_2)} - C_{\text{out}\,(CO_2)}} \times 100 \quad (3)$$

where $C_{in(CO_2)}$ and $C_{out(CO_2)}$ are the inlet and outlet concentrations, respectively; $C_{(CH_4)}$ is the methane concentration in the product. Furthermore, the turnover frequency (TOF) values corresponding to the reaction temperature of 200 °C were studied in the comparison of CH_4 yield for these Ni/TiO_2 catalysts. With the definition of the number of CH_4 molecules produced per Ni atom per second, the TOF of CH_4 yield was calculated as follows:

$$\text{TOF} = \frac{\text{the number of moles of } CH_4 \text{ produced per second}}{\text{the number of moles of surface Ni sites}} \quad (4)$$

where the number of moles of surface Ni sites was calculated based on the TPD results.

3. Result and discussion

3.1 Structural and morphological study of the catalysts

The XRD patterns of the as-calcined NiO/TiO_2 samples and P25 support are shown in Fig. 1A. For the pristine P25, characteristic reflections of titanium oxide (anatase: 25.3°, 37.8° and 53.9°; rutile: 27.9°, 36.4° and 55.1°) were observed (Fig. 1A, curve a), in agreement with the standard JCPDS diffraction pattern (see the bottom of Fig. 1A). After immobilization of Ni the species on P25 by the DP method, no obvious diffraction peaks assigned to NiO can be detected in all the as-calcined NiO/TiO_2-DP samples within the Ni loading range of 5–20 wt% (Fig. 1A, curve b–e). This can be explained by the small size of NiO particles in these DP samples. For the as-calcined

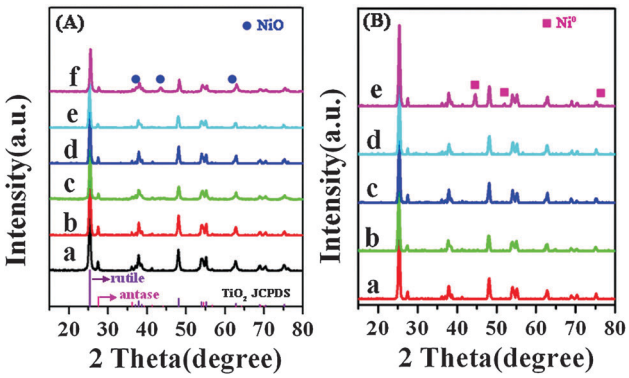

Fig. 1 (A) XRD patterns of the as-calcined samples: (a) P25, (b) NiO(5%)/TiO_2-DP, (c) NiO(10%)/TiO_2-DP, (d) NiO(15%)/TiO_2-DP, (e) NiO(20%)/TiO_2-DP, (f) NiO(15%)/TiO_2-IMP. The standard diffraction patterns of TiO_2 from JCPDS are shown at the bottom. (B) XRD patterns of the as-reduced catalysts: (a) Ni(5%)/TiO_2-DP, (b) Ni(10%)/TiO_2-DP, (c) Ni(15%)/TiO_2-DP, (d) Ni(20%)/TiO_2-DP, (e) Ni(15%)/TiO_2-IMP.

NiO(15%)/TiO_2-IMP sample (Fig. 1A, curve f), however, three reflections at 37.2°, 43.3° and 62.9° corresponding to (222), (400) and (440) of the face-centered cubic (fcc) NiO phase (JCPDS No. 89-5881) were observed, implying relatively larger NiO particles supported on TiO_2 by the IMP method. In addition, the XRD patterns of the as-reduced Ni/TiO_2 catalysts are shown in Fig. 1B. For the as-reduced Ni/TiO_2-DP catalysts, no diffraction peaks of metallic Ni can be observed in their XRD patterns (Fig. 1B, curve a–d), implying the metallic Ni NPs with a small size being immobilized on TiO_2. However, in the case of the as-reduced Ni(15%)/TiO_2-IMP catalyst, three reflections at 44.5°, 51.9° and 76.4° corresponding to (111), (200) and (220) of the fcc Ni phase (JCPDS No. 87-0712) can be identified, which suggests that the supported Ni NPs by the IMP method possess a larger particle size than deposited by DP method.

Fig. 2 shows the H_2-TPR profiles of the as-calcined Ni/TiO_2 samples. For the Ni(5%)/TiO_2-DP sample, only one distinct peak at 453 °C was observed. As the Ni loading was increased from 10 to 20 wt%, another peak appears at a lower temperature of 300 °C. Based on previously reported work,[41–44] the peak

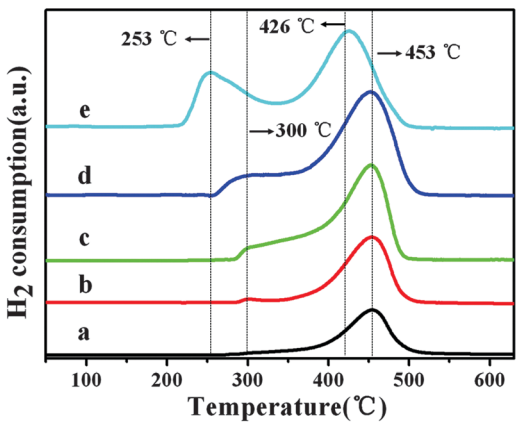

Fig. 2 H_2-TPR profiles of (a) NiO(5%)/TiO_2-DP, (b) NiO(10%)/TiO_2-DP, (c) NiO(15%)/TiO_2-DP, (d) NiO(20%)/TiO_2-DP and (e) NiO(15%)/TiO_2-IMP.

at the lower temperature is assigned to the reduction of bulk NiO which interacts weakly with TiO_2; while the higher temperature peak is attributed to the reduction of highly-dispersed NiO species with strong bonding to the TiO_2 support. Moreover, it should be noted that the intensity ratio between the low-temperature peak and the high-temperature peak (I_L/I_H) increases gradually with the increase of Ni loading, indicating the enhancement of the bulk NiO phase in the samples. However, for the Ni(15%)/TiO_2-IMP sample, two distinct peaks appear at 253 °C and 426 °C, respectively, much lower than those of the Ni(15%)/TiO_2-DP sample, implying a relatively weaker interaction between NiO and TiO_2. In addition, the significantly higher I_L/I_H ratio of the Ni(15%)/TiO_2-IMP sample suggests a lower dispersion of NiO species on the surface of the TiO_2.

The TEM images of all the as-reduced Ni/TiO_2 samples clearly reveal the change in particle size of the supported Ni with various Ni loadings. With the increase of Ni loading, the Ni particle size increases from ~1.5 nm (Ni(5%)/TiO_2-DP) to ~2.6 nm (Ni(20%)/TiO_2-DP) (Fig. 3a–d). The sample of Ni(15%)/TiO_2-DP displays a particle size of ~2.2 nm, much smaller than that of the Ni(15%)/TiO_2-IMP sample (5.8 nm, Fig. 3e). A high-resolution TEM image for Ni(15%)/TiO_2-IMP (Fig. 3f) reveals the single crystalline metallic Ni. The fringes with a lattice spacing of 0.204 nm can be indexed to the (111) plane of face-centered Ni. Therefore, the comparison between the TEM image of Ni(15%)/TiO_2-DP (Fig. 3c) and Ni(15%)/TiO_2-IMP (Fig. 3e) demonstrates the highly-dispersed Ni NPs with smaller particle size in the former catalyst.

3.2 Evaluation of the catalytic behavior

The catalytic activities of the obtained Ni/TiO_2-DP catalysts towards the reaction of CO_2 methanation were studied. Fig. 4A shows the CO_2 conversion as a function of temperature at a reaction GHSV of 2400 h^{-1}. The value of T_{50}, corresponding to the temperature at which a conversion of 50% is obtained, was 218 °C (Ni(15%)/TiO_2-DP and Ni(20%)/TiO_2-DP), 234 °C (Ni(10%)/TiO_2-DP) and 246 °C (Ni(5%)/TiO_2-DP), respectively, much lower than that of Ni(15%)/TiO_2-IMP (276 °C). It was found that the catalytic activity of the Ni/TiO_2-DP samples increases with the enhancement of Ni loading from 5 to 15 wt%, and almost remains the same with further increase of the Ni loading from 15 to 20 wt%. The sample of Ni(15%)/TiO_2-DP exhibits a significantly improved low-temperature activity towards CO_2 methanation. The CO_2 conversion reaches up to 96.0% at the temperature of 260 °C, which is close to the thermodynamic maximum value at this temperature (the dotted line in Fig. 4A)[20] and far superior to the catalytic activity of supported Ni catalysts reported previously.[9,26,27] Moreover, it should be noted that the Ni(15%)/TiO_2-DP catalyst also shows a very satisfactory selectivity towards CH_4 (99%) over the whole temperature range (Fig. 4B). In the presence of the Ni(15%)/TiO_2-IMP sample, however, the maximum CO_2 conversion of

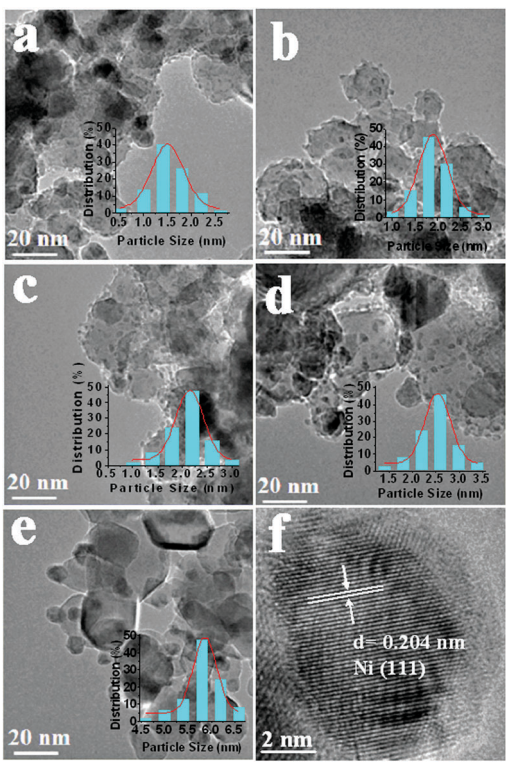

Fig. 3 (A) TEM images of Ni/TiO_2 after reduction at 450 °C for 4 h: (a) Ni(5%)/TiO_2-DP, (b) Ni(10%)/TiO_2-DP, (c) Ni(15%)/TiO_2-DP, (d) Ni(20%)/TiO_2-DP, (e) Ni(15%)/TiO_2-IMP, (f) HRTEM for Ni(15%)/TiO_2-IMP. Corresponding Ni particle size distribution is shown in the inset.

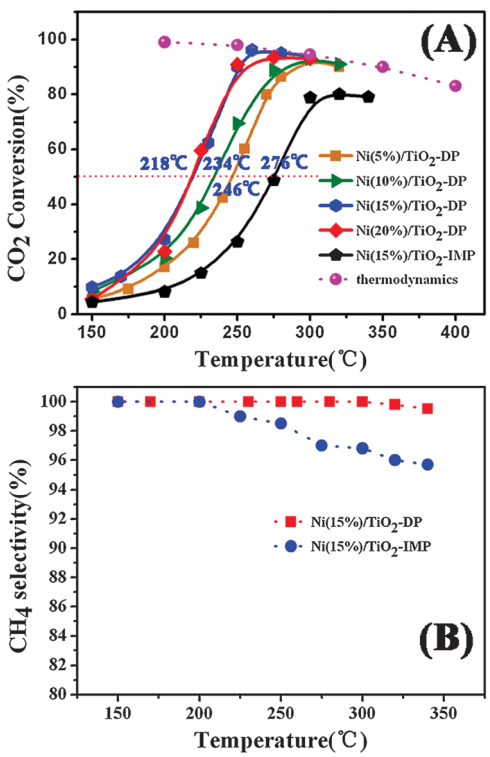

Fig. 4 (A) CO_2 conversion *vs.* temperature for Ni(5%)/TiO_2-DP, Ni(10%)/TiO_2-DP, Ni(15%)/TiO_2-DP, Ni(20%)/TiO_2-DP, and Ni(15%)/TiO_2-IMP. (B) CH_4 selectivity *vs.* temperature for Ni(15%)/TiO_2-DP and Ni(15%)/TiO_2-IMP.

80.1% was obtained at a high temperature of 340 °C, with a selectivity of 95%. The results demonstrate that the Ni(15%)/TiO_2 catalyst prepared by the DP method displays significantly enhanced low-temperature activity and selectivity in comparison with the conventional IMP method, which will be further discussed in the next section.

The conversion of CO_2 as a function of GHSV (1800–9000 h^{-1}) at the corresponding maximum conversion temperature for Ni(15%)/TiO_2-DP and Ni(15%)/TiO_2-IMP, respectively, is shown in Fig. 5. The results show that the CO_2 conversion (96%) over the Ni(15%)/TiO_2-DP catalyst at 260 °C almost remains unchanged upon increasing the GHSV, while the conversion over Ni(15%)/TiO_2-IMP at 340 °C decreases gradually from 81.5% to 65.0%. Moreover, catalytic stability tests of Ni(15%)/TiO_2-DP and Ni(15%)/TiO_2-IMP were carried out on stream for 81 h at their maximum conversion temperature (260 °C and 340 °C, respectively), with a GHSV of 2400 h^{-1} (Fig. S1, ESI†). The results show that the Ni(15%)/TiO_2-IMP catalyst suffers from a large activity loss, from 80.1% to 69.2%. In contrast, the Ni(15%)/TiO_2-DP sample exhibits good catalytic stability, with CO_2 conversion decreasing only slightly, from 96% to 93.2%. In addition, the turnover frequency (TOF) towards methane at 200 °C was calculated and is shown in Table 1. For the Ni/TiO_2-DP catalysts, the increase of Ni loading leads to the enhancement of the total active sites and the resulting CO_2 conversion (catalytic activity); however, the enlarged Ni particles cause a decrease in the activity of the surface Ni atoms. As a result, the TOF value in Table 1 decreases along with the increase of Ni loading under the same condition of GHSV. It is worth noting that with the same Ni loading, the Ni(15%)/TiO_2-DP catalyst displays a larger TOF value (1.22×10^{-3} s^{-1}) than that of the Ni(15%)/TiO_2-IMP catalyst (7.26×10^{-4} s^{-1}), indicating a higher activity of Ni(15%)/TiO_2-DP towards CO_2 methanation at low temperature.

3.3 Discussion

To clarify the driving force for the formation of highly-dispersed Ni NPs on the surface of TiO_2 prepared by the DP method, XPS was used to characterize the chemical environment of Ni species from the Ni(15%)/TiO_2 samples before calcination. Fig. 6 shows the binding energy of Ni $2p_{3/2}$ for the Ni(15%)/TiO_2-DP precursor is 855.4 eV (curve b), which is lower than that of nickel hydroxide (855.8 eV, curve a). This indicates that an interaction may occur between the Ni^{2+} species precursor and the TiO_2 substrate in the DP process. Since the solution pH is above the point of zero charge of amphoteric TiO_2 (PZC_{TiO_2}: ~6)[45] during the DP synthesis process, Ni^{2+} species can interact with the deprotonated surface of TiO_2 *via* an analogous Ni–O–Ti bond, accounting for the decrease in the Ni $2p_{3/2}$ binding energy compared with that of nickel hydroxide. A similar phenomenon in the Au–TiO_2 system has also been reported in that one $Au(en)_2^{3+}$ cation interacts with $3O^-$ of the deprotonated surface of TiO_2.[46] In the case of the Ni(15%)/TiO_2-IMP precursor sample, a binding energy of Ni $2p_{3/2}$ at 854.9 eV was observed (curve d), which is in accordance with that of nickel nitrate (curve c). The above results indicate that different Ni precursors were formed by using the different preparation methods. Both the results of TEM and H_2-TPR show that a high dispersion of supported Ni NPs can be obtained by employing the DP method, owing to the interaction between Ni^{2+} species and the deprotonated surface of TiO_2 in the DP process.

H_2-TPD was performed to give further insight into the effect of dissociative hydrogenation on the reaction activity of the

Table 1 Structural parameters of Ni/TiO_2 catalysts and their methanation activity

Samples	S_{BET}/ m^2 g^{-1}	Ni[a] (wt%)	Ni dispersion[b] (%)	Mean Ni particle size by TEM/nm	TOF[c] of CH_4 at 200 °C/s^{-1}
TiO_2	56.7	—	—	—	—
Ni(5%)/TiO_2-DP	56.2	4.89	43.0	1.5 ± 0.3	2.14×10^{-3}
Ni(10%)/TiO_2-DP	55.8	9.91	40.3	1.8 ± 0.4	1.33×10^{-3}
Ni(15%)/TiO_2-DP	54.9	14.82	39.5	2.1 ± 0.4	1.22×10^{-3}
Ni(20%)/TiO_2-DP	53.9	16.76	38.2	2.6 ± 0.5	9.33×10^{-4}
Ni(15%)/TiO_2-IMP	50.5	14.93	19.7	5.8 ± 0.8	7.26×10^{-4}

[a] Value determined by ICP. [b] Value calculated based on the H_2-TPR and H_2-TPD results. [c] The TOF value was calculated based on the metal dispersion and the yield of CH_4 at 200 °C.

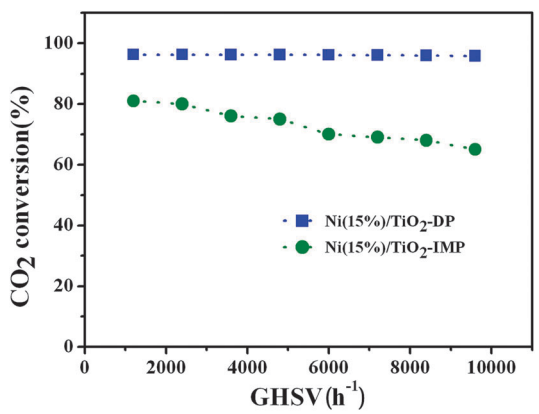

Fig. 5 CO_2 conversion *vs.* GHSV for the Ni(15%)/TiO_2-DP and Ni(15%)/TiO_2-IMP catalyst, respectively.

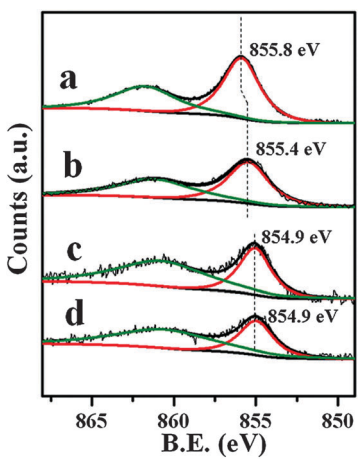

Fig. 6 Ni 2p XPS of (a) $Ni(OH)_2$, (b) Ni(15%)/TiO_2-DP before calcination, (c) $Ni(NO_3)_2$ and (d) Ni(15%)/TiO_2-IMP before calcination.

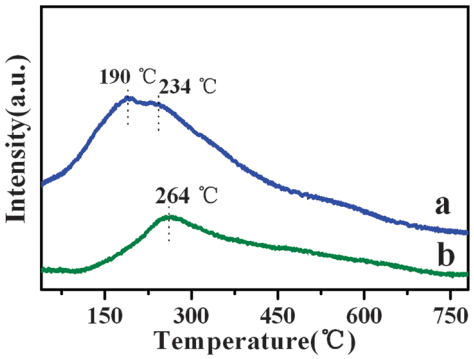

Fig. 7 (A) H_2-TPD profiles of (a) Ni(15%)/TiO_2-DP and (b) Ni(15%)/TiO_2-IMP.

Ni/TiO_2 catalysts (Fig. 7). For the sample of Ni(15%)/TiO_2-DP, two peaks were observed at 190 °C and 234 °C in the H_2-TPD profile, respectively. The peak at the lower temperature (190 °C) can be attributed to hydrogen chemisorbed at the surface of highly-dispersed Ni NPs with a large density of surface defects. It was reported the surface defects can serve as capture traps for surface hydrogen diffusion which reduces the activation energy of hydrogen dissociation.[34–37] In contrast to the former desorption peak, the higher temperature peak (234 °C) is attributed to hydrogen adsorbed at bulk or poorly-dispersed Ni NPs. In the case of Ni(15%)/TiO_2-IMP, however, its TPD profile is characterized by only one peak located at 264 °C, which can be attributed to hydrogen chemisorbed at the surface of bulk Ni. Moreover, it should be noted that the Ni(15%)/TiO_2-DP sample shows a relatively lower desorption temperature with much stronger intensity, in comparison with that of Ni(15%)/TiO_2-IMP, demonstrating that the Ni(15%)/TiO_2-DP sample has a higher Ni dispersion and more surface-dissociated hydrogen can be generated on this sample.

In addition, the surface structure of Ni(15%)/TiO_2-DP and Ni(15%)/TiO_2-IMP were investigated by EXAFS spectroscopy (Fig. 8). The fitting parameters (Table 2) show that both the Ni–Ni coordination numbers of the two catalysts are less than that of Ni foil (12). Moreover, it should be noted that the fresh Ni(15%)/TiO_2-DP catalyst exhibits a lower Ni–Ni coordination

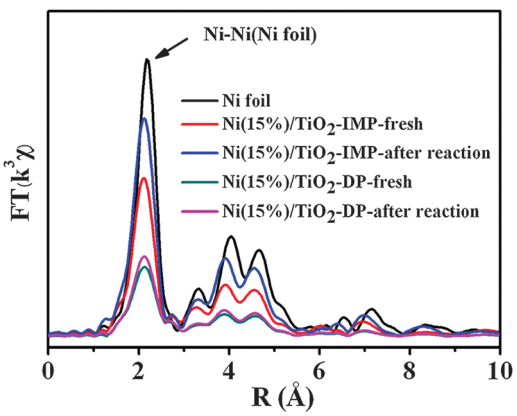

Fig. 8 Fourier transforms of EXAFS spectra for Ni foil, fresh Ni(15%)/TiO_2-DP, fresh Ni(15%)/TiO_2-IMP and the two catalysts after reaction.

Table 2 EXAFS fitting parameters of Ni foil, Ni(15%)/TiO_2-DP and Ni(15%)/TiO_2-IMP before and after reaction[a]

Samples	*N*	*R*/Å
Ni foil	12	2.50
Ni(15%)/TiO_2-IMP-fresh	7.5	2.49
Ni(15%)/TiO_2-IMP-after reaction	10.5	2.49
Ni(15%)/TiO_2-DP-fresh	5.8	2.49
Ni(15%)/TiO_2-DP-after reaction	6.1	2.49

[a] *N* = coordination number. Error bounds (accuracies) characterizing the structural parameters obtained by EXAFS spectroscopy are estimated to be as follows: coordination number *N*, ±20%; distance *R*, ±0.02 Å.

number (5.8) than that of fresh Ni(15%)/TiO_2-IMP (7.5), *i.e.*, the former catalyst has a higher unsaturation of Ni–Ni coordination than the latter. Combined with the above TPD results, it can therefore be speculated that more active sites/defects exist in the Ni(15%)/TiO_2-DP sample resulting from the higher unsaturation of Ni species, which accelerates the dissociated-surface hydrogen[32,33] and contributes to the promotion of its low-temperature activity. In addition, it can be seen from Table 2 that for the Ni(15%)/TiO_2-IMP sample, a significant increase in the Ni–Ni coordination number was observed (from 7.5 to 10.5) after the reaction for 81 h. This is responsible for the obvious activity loss of Ni(15%)/TiO_2-IMP (Fig. S1, ESI†). In contrast, only a slight increase in the Ni–Ni coordination number was observed (from 5.8 to 6.1) for the Ni(15%)/TiO_2-DP catalyst after reaction, indicating a high activity for long-term use. This is further confirmed by TEM images of the two used catalysts. Fig. S2 (ESI†) shows that the particle size and morphology of the Ni NPs in the Ni(15%)/TiO_2-DP catalyst remain almost unchanged after reaction for 81 h on stream, while obvious agglomeration was clearly observed in the Ni(15%)/TiO_2-IMP sample.

4. Conclusions

The hydrogenation of carbon dioxide to methane was performed over Ni/TiO_2 catalysts. Superior behavior with a carbon dioxide conversion of 96% and selectivity of 99% was obtained over the Ni(15%)/TiO_2-DP catalyst at a low temperature (260 °C). This catalyst is structurally stable after long-term use and shows excellent catalytic stability under the relatively mild conditions. Characterisation studies based on XRD, H_2-TPR and XPS reveal that the highly-dispersed Ni precursor can be formed during the DP process, which subsequently contributes to the formation of a supported catalyst with a high metallic Ni dispersion. H_2-TPD and EXAFS results demonstrate that supported Ni NPs possess a high unsaturation, which may lead to the enhanced exposure of active sites that facilitate the generation of surface-dissociated hydrogen, accounting for the excellent low-temperature activity of the Ni(15%)/TiO_2-DP catalyst. Therefore, this work provides a facile method for the preparation of a supported Ni catalyst with high dispersion, and demonstrates its largely enhanced low-temperature activity for carbon dioxide methanation. It is expected that this strategy

can be extended for the fabrication of other metal heterogeneous catalysts with significantly improved behavior.

Acknowledgements

This work was supported by the 973 Program (Grant No. 2011CBA00504) and the National Natural Science Foundation of China (NSFC). M.W. particularly appreciates the financial aid from the China National Funds for Distinguished Young Scientists of the NSFC.

Notes and references

1 X. D. Xu and J. A. Moulijin, *Energy Fuels*, 1996, **10**, 305–325.
2 U. Phairat, M. Dena, V. Amornvadee and T. Paitoon, *Ind. Eng. Chem. Res.*, 2006, **45**, 2558–2568.
3 N. S. Spinner, J. A. Vega and W. E. Mustain, *Catal. Sci. Technol.*, 2012, **2**, 19–28.
4 W. Wang, S. P. Wang, X. B. Ma and J. L. Gong, *Chem. Soc. Rev.*, 2011, **40**, 3703–3727.
5 C. Y. Zhao, L. J. Liu, Q. Y. Zhang, J. Wang and Y. Li, *Catal. Sci. Technol.*, 2012, **2**, 2558–2568.
6 A. Bansode, B. Tidona, P. R. Rohr and A. Urakawa, *Catal. Sci. Technol.*, 2013, **3**, 767–778.
7 Q. Zhang, Y. Z. Zuo, M. H. Han, J. F. Wang, Y. Jin and F. Wei, *Catal. Today*, 2010, **150**, 55–60.
8 (*a*) P. Gao, F. Li, F. K. Xiao, N. Zhao, N. N. Sun, W. Wei, L. S. Zhong and Y. H. Sun, *Catal. Sci. Technol.*, 2012, **2**, 1447–1454; (*b*) W. N. Wang, J. Park and P. Biswas, *Catal. Sci. Technol.*, 2011, **1**, 593–600.
9 J. N. Park and E. W. Mcfarland, *J. Catal.*, 2009, **266**, 92–97.
10 T. Abe, M. Tanizawa, K. Watanabe and A. Taguchi, *Energy Environ. Sci.*, 2009, **2**, 315–321.
11 L. T. Luo, S. J. Li and Y. Zhu, *J. Serb. Chem. Soc.*, 2005, **70**, 1419–1425.
12 M. Kusmierz, *Catal. Today*, 2008, **137**, 429–432.
13 Z. Kowalczyk, K. Stolecki and W. Rarog-Pilecka, *Appl. Catal., A*, 2008, **342**, 35–39.
14 T. Szailer, E. Novak, A. Oszko and A. Erdohelyi, *Top. Catal.*, 2007, **46**, 79–86.
15 E. I. Papaioannou, S. Souentie, A. Hammad and C. G. Vayenas, *Catal. Today*, 2009, **146**, 336–344.
16 R. D. Hetterley, R. Mackey, J. T. A. Jones, Y. Z. Khimyak, A. M. Fogg and L. V. Kozhevnikov, *J. Catal.*, 2008, **258**, 250–255.
17 Y. Q. Lang, Q. Q. Wang, J. M. Xing, B. Zhang and H. Z. Liu, *AIChE J.*, 2008, **54**, 2303–2309.
18 Q. Wang and D. O'Hare, *Chem. Rev.*, 2012, **112**, 4124–4155.
19 M. Wei, X. Zhang, D. G. Evans, X. Duan, X. J. Li and H. Chen, *AIChE J.*, 2007, **53**, 2916–2924.
20 F. Ocampo, B. Louis and A. C Roger, *Appl. Catal., A*, 2009, **369**, 90–96.
21 X. Xiang, L. Bai and F. Li, *AIChE J.*, 2010, **56**, 2934–2945.
22 R. Razzaq, H. W. Zhu, L. Jiang, U. Muhammad, C. S. Li and S. J. Zhang, *Ind. Eng. Chem. Res.*, 2013, **52**, 2247–2256.
23 F. W. Chang, T. J. Hsiao and J. D. Shih, *Ind. Eng. Chem.Res.*, 1998, **37**, 3838–3845.
24 F. W. Chang, M. S. Kuo, M. T. Tsay and M. C. Hsieh, *Appl. Catal., A*, 2003, **247**, 309–320.
25 M. Yamasaki, H. Habazaki, K. Asami, K. Izumiya and K. Hashimoto, *Catal. Commun.*, 2006, **7**, 24–28.
26 N. Perkas, G. Amirian, Z. Y. Zhong, J. Teo, Y. Gofer and A. Gedanken, *Catal. Lett.*, 2009, **130**, 455–462.
27 G. D. Lee, M. J. Moon, J. H. Park, S. S. Park and S. S. Hong, *Korean J. Chem. Eng.*, 2005, **22**, 541–546.
28 J. Sehested, K. E. Larsen, A. L. Kustov, A. M. Frey, T. Johannessen, T. Bligaard, M. P. Andersson, J. K. Norskov and C. H. Christensen, *Top. Catal.*, 2007, **45**, 9–13.
29 S. Sane, J. M. Bonnier, J. P. Damon and J. Masson, *Appl. Catal.*, 1984, **9**, 69–83.
30 M. Agnelli, M. Kolb and C. Mirodatos, *J. Catal.*, 1994, **148**, 9–21.
31 S. J. Choe, H. J. Kang, S. J. Kim, S. B. Park, D. H. Park and D. S. Huh, *Bull. Korean Chem. Soc.*, 2005, **26**, 1682–1688.
32 (*a*) M. Chen, Z. Z. Cai, X. B. Yang, M. Zhu and Y. J. Zhao, *Surf. Sci.*, 2012, **606**, 45–49; (*b*) V. H. Pieter, V. D. B. Jan-Albert and L. M. Ciobîcă, *Catal. Sci. Technol.*, 2012, **2**, 491–494.
33 D. C. Hu, J. J. Gao, P. Yuan, H. J. Li, G. W. Poernomo, Z. Y. Zhong, G. G. Xu, F. N. Gu and F. B. Su, *Ind. Eng. Chem. Res.*, 2012, **51**, 4875–4886.
34 H. P. Van, B. Vanden, A. Jan and C. J. Weststrate, *ACS Catal.*, 2012, **2**, 1097–1107.
35 M. H. Weng, H. T. Chen, Y. C. Wang, S. P. Ju, J. G. Chang and M. C. Lin, *Langmuir*, 2012, **28**, 5596–5605.
36 G. X. Li, X. W. Chen, J. D. Bai, Z. Q. Lan and J. Guo, *Acta. Phys.–Chim. Sin.*, 2010, **26**, 1448–1456.
37 M. Kong, Y. Li, X. Chen, T. Tian, P. Fang, F. Zheng and X. Zhao, *J. Am. Chem. Soc.*, 2011, **133**, 16414–16417.
38 (*a*) G. Ouyang, W. G. Zhu, G. W. Yang and Z. M. Zhu, *J. Phys. Chem. C*, 2010, **114**, 4929–4933; (*b*) Z. L. Wang, *Characterization of Nanophase Materials*, Wiley-VCH Verlag GmbH, Weinheim, Germany, 2001.
39 S. He, C. M. Li, H. Chen, D. S. Su, B. S. Zhang, X. Z. Cao, B. Y. Wang, M. Wei, D. G. Evans and X. Duan, *Chem. Mater.*, 2013, **25**, 1040–1046.
40 F. Z. Zhang, J. L. Chen, P. Chen, Z. Y. Sun and S. L. Xu, *AIChE J.*, 2012, **58**, 1853–1861.
41 B. Mile, D. Stirling, M. A. Zammitt, A. Lovell and M. Webb, *J. Catal.*, 1988, **114**, 217–229.
42 V. M. Shinde and G. Madras, *Appl. Catal., B*, 2013, **132**, 28–38.
43 X. L. Yan, Y. Liu, B. R. Zhao, Z. Wang, Y. Wang and C. J. Liu, *Int. J. Hydrogen Energy*, 2013, **38**, 2283–2291.
44 C. Zhao, Y. Z. Yu, A. Jentys and J. A. Lercher, *Appl. Catal., B*, 2013, **132**, 282–292.
45 S. Tsubota, D. A. H. Cunningha, Y. Bando and M. Haruta, *Stud. Surf. Sci. Catal.*, 1995, **91**, 227–235.
46 R. Zanella, L. Delannoy and C. Louis, *Appl. Catal., A*, 2005, **291**, 62–72.